Chapter III

Surface roughness mediated-wettability and reflectance characteristics of dragonfly and damselfly wings

In nature, noticeable wetting-dewetting responses can be witnessed in numerous insects, like water strider, beetle, moth, butterfly, dragonfly, damselfly etc. Accordingly, a large class of insects, moths and flies fly in the rain without getting wet owing to their structurally impermeable wings. The dewetting response of these insect wings is believed to alter with the surface construction and microscopic geometry there in, thus giving rise to a very high water CA. In particular, almost all dragonflies could make their uninterrupted flight in the rain without getting wet [1]. Exploiting the non-wetting property of dragonfly wings is of fundamental interest for directing research towards making suitable artificial surfaces of select morphology and microstructure. In the past, the wettability of a dragonfly wing was considered largely due to its waxy cuticular surfaces [2,3]. The stenocara beetle found in the Namib desert could collect drinking water from the fog-laden wind on their backs. These droplets are formed by the insect's bumpy surface, which consists of alternate hydrophobic (wax-coated) and hydrophilic (non-waxy) regions [4]. The water strider's legs show good water repellent property due to its unique microstructural patterns, for which water CA is as high as ~167° [5]. The butterfly wings too, exhibit hydrophobic characteristics on which water drops can move freely along slanted direction. The wettability of pigeon feather has also been worked out with the proposition that the Cassie-Baxter wetting regime is inherent in the pigeon pennae [6, 7]. A two-fold hierarchical pattern comprising of barbs and barbules was believed to be mainly responsible for displaying larger CA values and consequently, remarkable water repellency.

While evaluating wetting-dewetting phenomena, the nature of surface roughness is typically assessed for all types of above mentioned species. The Wenzel model is generally employed to characterise the collapsed state of the drop on a surface structure, whereas suspended state of the drop is dictated by the Cassie-Baxter model [2,7]. It is not known, however, the limit of CA that predicts any departure from the condition of a smooth-flat surface while working with both the models, simultaneously. On the other hand, vizualizing

surface roughness both by CA and reflectance/transmittance measurements is rarely discussed in the literature. In this work, considering wings of the dragonfly and river blue damselfly wings as the test-bed, we exploit dewetting behavior of the specimens while moving from one region to the other across the wing surface. It is worth mentioning here that, both the specimen types belong to the same order, namely, *Odanata*. The specimens are special in the sense that, dragonfly wings are kept fully extended and stay flat away from the body when at rest, while the damselfly wings are held back together across the body crossed. Unlike many other insects, a dragonfly is fully dependent on its wings for movement since it cannot walk with the help of legs. Usually, the time of flight of the dragonfly species is comparatively larger than that of the damselfly counterpart.

This chapter demonstrates dewetting and reflectance responses of the aforesaid specimens with the help of experimental data and simple theoretical treatment.

3.1 Specimen collection and sectioning

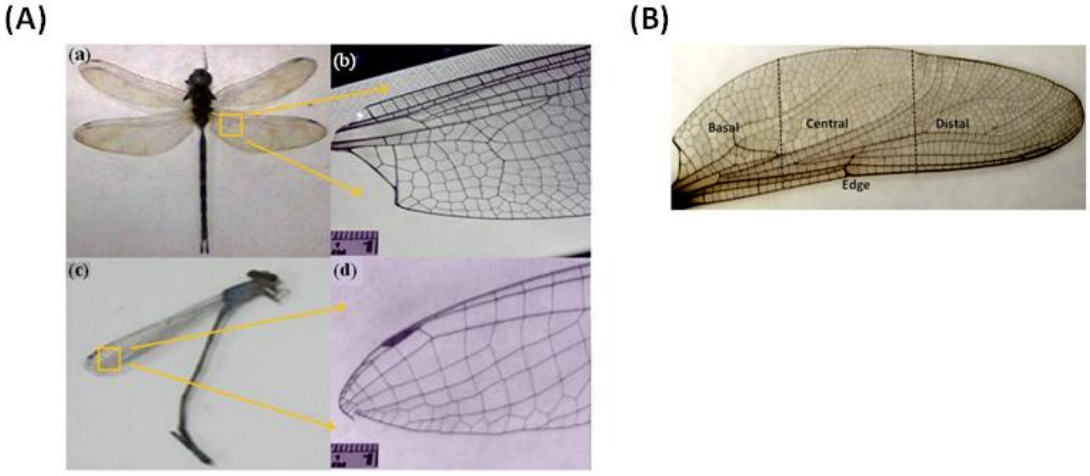

Fig. 3.1 (A) (a) Digital photograph of the dragonfly (Gynacantha Dravida). An enlarged, microscopic view of the hind-wing is imaged by a 10× digicam, shown in (b). The digital and microscopic images of the hind-wing of the blue riverdamselfly are presented in (c) and (d); respectively. The scale bar shown in (b) and (d) represents 2 mm (B) Schematic representation of basal, central and distal parts of dragonfly wing.

The investigated specimens are basically the hindwings of a matured female dragonfly acquired from one of our University garden during post-monsoon season prevailing in the NE India (Fig.3.1). The sample dragonflies (*Gynacantha Dravida*) belongs to the family of *Aeshnidae* and order *Odanata* and is reported to be found in the western ghat, eastern and north-eastern regions of Indian sub-continent [8]. The abdomen of the dragonfly is nearly 4.4 cm long, while respective length and breadth of the wings are found as, ~4.5 cm and 1.5 cm (Fig. 3.1(a)). The enlarged view of the hind wing is acquired through 10× microscopic imaging, shown in Fig. 3.1(b). The sub-figure illustrates a great variety of polygons, both in size and shape as one moves along the length and across the breadth. The other specimen considered was a blue riverdamselfly (*Pseudagrion Microcephalum*) and belonging to the family *Coenagrionidae*, of order *Odanata* and suborder *Zygoptera*. The digital and 10× microscopic photographs of the wing are depicted in Fig. 3.1(c) and (d); respectively.

Although in some earlier works chemically treated wings are employed in order to minimize the time dependent changes of the surface properties [9], here the samples are left untreated to restore the chemical and physical properties of the cuticle and waxy layer as they are. The portion of the wing close to the abdomen is recognized as the basal part, while the region away from the abdomen is termed as the distal part. Shown schematically in Fig. 3.1 (B), the basal, central, distal and edge parts of the dragonfly hindwing are shown. Both dragonfly and damselfly hindwings were examined and analyzed with the help of CA and reflectance measurements, as per requirement.

3.2 Morphological analysis of the dragonfly and blue river-damselfly wings

Fig. 3.2(A)(a-d) shows the SEM micrographs of the dragonfly and damselfly wings. The microstructural network of both the wing types was found to comprise of a number of closed regions with cage-like morphologies. The surface construction of the wing consists of polygonal makeups which appear in the form of rectangular, pentagonal and hexagonal units or combination of

these. Each of the microstructure regions of the dragonfly wing is entrapped by five to six chitinous fibres that result in pentagonal and hexagonal structures (Fig. 3.2(A)(a)). In contrast, square/rectangular-shaped morphology can be revealed as regards the hindwing of the blue river damselfly (Fig. 3.2(A)(c)). This can be attributed to the fact that the dragonfly wing microstructure network has three-end junctions (shown by red arrows), whereas the damselfly wing structure contained four-end junctions (shown by blue arrows). The average span area of the polygonal unit is approximately, ~105
μm^2. Each of the polygonal regions is bound by several hundred, micron size long (200–700 μm) chitin-based fibres, having an average thickness of ~21 μm and ~12 μm, as for the dragonfly and damselfly cases (Fig. 3.2(A)(a,c)). Occasionally, the side-fibres of the enclosed region contained short ridges that give thorn like appearances. This feature is, however, more prominent in the dragonfly specimen, whereas damselfly specimen showed uniformly spaced bright spots on the side-edges, which may indicate broken positions of the thorns. We observe that the number of whole polygons increase as we move from the basal to the distal region (Fig. 3.2(B)(a-c)). Moreover, the triple junctions in all these three regions vary from one another. They are either Y-shaped or, T-shaped, but appear with varying dimensions. Some of them are perfectly T-shaped *i.e.*, the angle between the fibre-stems is 90°, whereas the Y-shaped ones are characterized by at least one obtuse angle. Essentially, the interior area of a polygon has a *2d* membrane like planar architecture. At a higher magnification, we noticed the existence of randomly distributed oblate and rod- shaped units with tip-end diameters in the range of ~100–125 nm, as evident from the figure inset (Fig. 3.2(A)(b,d)). The damselfly specimen seems to have more extended regions unoccupied by the chitin-oblates. The filled region of the damselfly specimen is however similar to the dragonfly species (Fig. 3.2(A)(d)). At a higher magnification, the chitinous oblates were observed to be more tilted with occasional airgaps in the basal part (Fig. 3.2(B)(d)–(f)). With pronounced packing characteristics, the packing density of the nanofibrils experienced by the distal

part (~72/mm^2) is substantially higher than that of the basal section (~43/mm^2). The chitinous nanofibrils tend to spread in the central region while offering a moderate packing density of ~50/mm^2. The overall spread of the chitinous nano-oblates, to a great extent, gives the impression of silt-filled black-tap road when viewed from a closer distance. It is important to note that, the mechanical strength and the flatness of typical wings are largely dependent on the nature of packing and polygonal microstructural design available in the wing part.

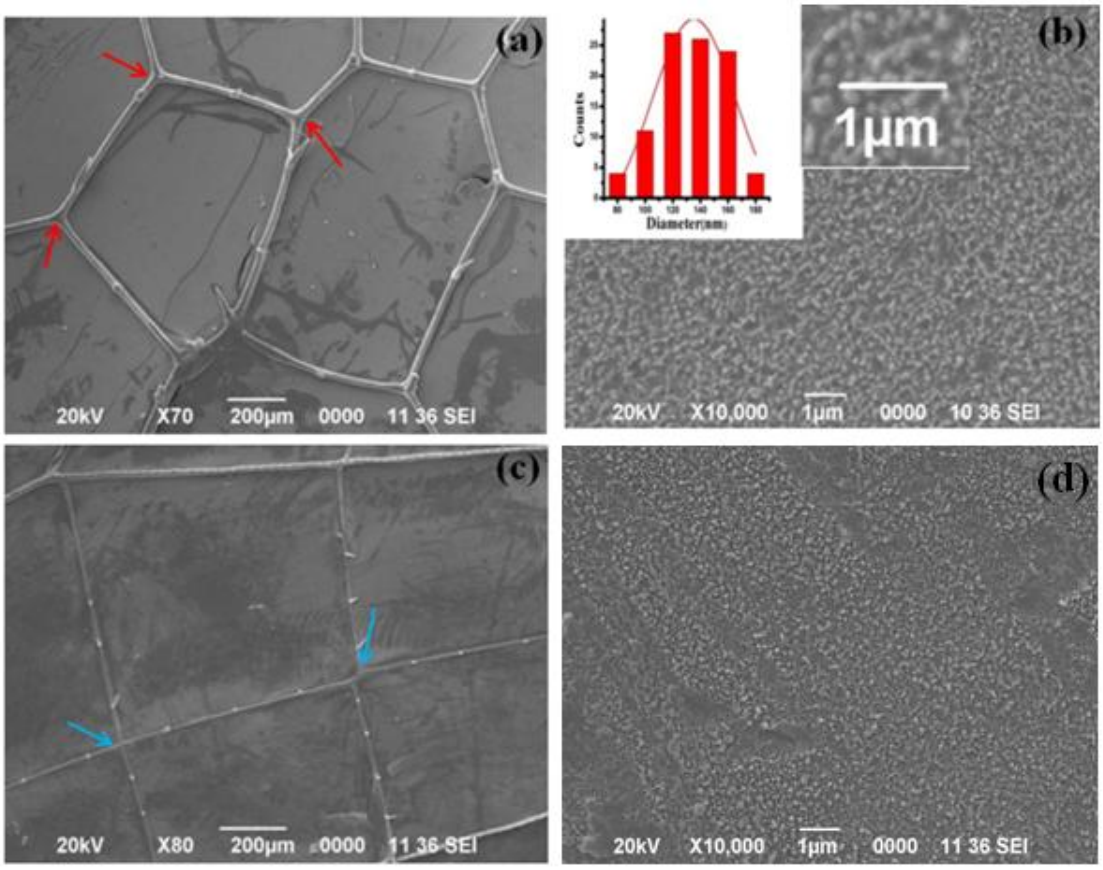

Figure 3.2 (A): SEM images of the central parts of (a,b) dragonfly wing and (c,d) damselfly wing. At a low magnification, microstructural polygonal network with triple (red arrow) and square (blue arrow) junctions are indicated in (a) and (c). The nano-oblate shaped randomly distributed fibrils present in the entrapped (polygonal) region are shown at (b) and (d). The inset is a histogram which depicts distribution of chitin-oblates with varying tip-end diameter.

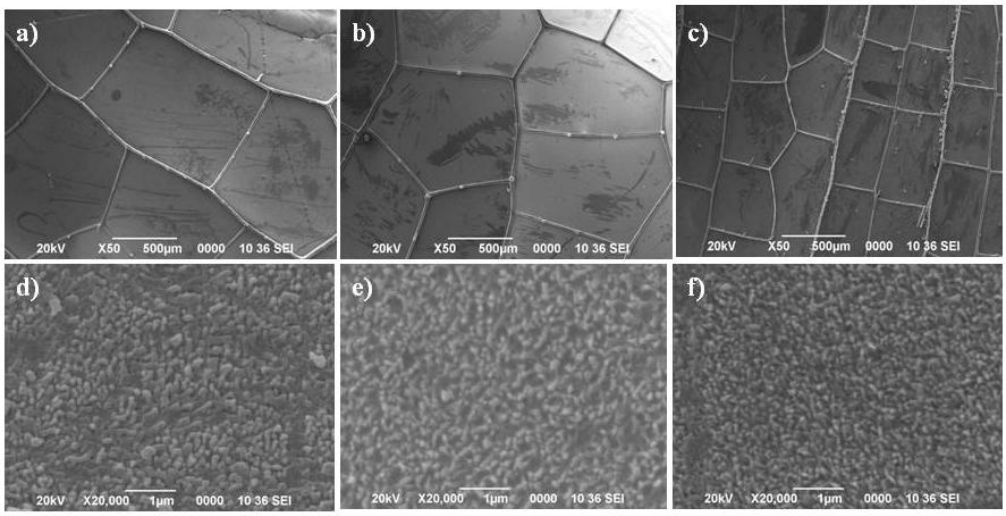

Figure 3.2 (B): SEM micrographs of (a) basal (b) central and (c) distal parts of the dragonfly hindwing captured at a lower magnification (upper panel). The magnified images are shown in sub-figures (d–f); respectively (lower panel).

3.3 Wettability studies on the hind-wing parts

Fig. 3.3 shows the digital images of water droplets on different parts of the wing surfaces, considering three parts, namely, basal (close to the insect body), central and distal (farthest from the insect body). Consequently, the water CAs are measured in the vicinity of the indicated parts both for the dragonfly and

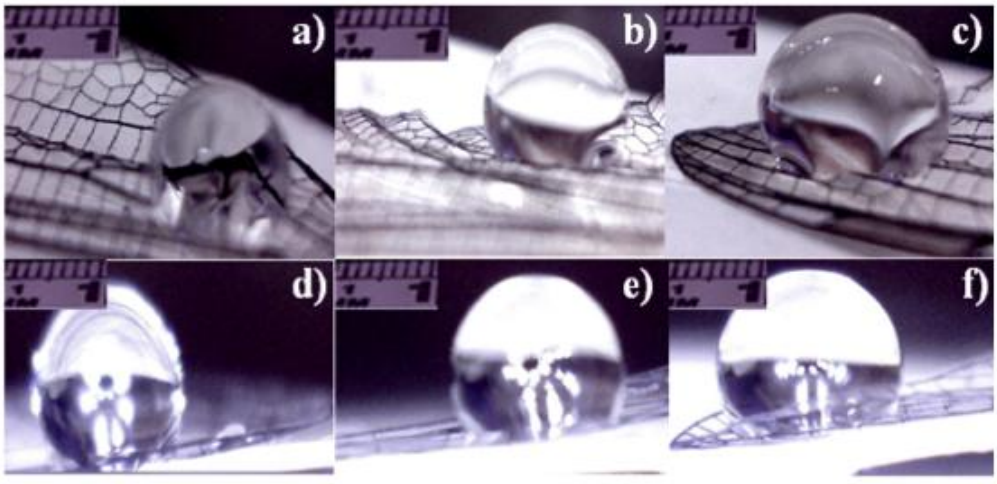

Figure 3.3: The side view of the water droplets sitting on different parts of the hind-wing of the (a–c) dragonfly and (d–f) damselfly specimens. The basal, central and distal regions corresponded to (a,d), (b,e), and (c,f); respectively. The scale bar shown in each of the images corresponds to 2 mm.

damselfly wings, repetitively. The side view of different parts holding droplets can be found in Fig. 3.3 and accordingly, measured angles are presented in Table 3.1. The wing surface, as one moves from the basal to the distal regions, suggests a varying hydrophobic response giving a water CA > 90◦. The measured CA values are in the range of 120–136° and is well below the superhydrophobic criterion (CA ≥ 150◦) [10]. According to Wenzel, the homogenously developed cuticle wax surface is primarily responsible for the hydrophobicity of the wing [10]. Although the nature of hydrophobicity is influenced by a number of factors, mainly chemical composition and surface morphology play dominant roles. The distal part is observed to be more hydrophobic with respect to both the basal and central segments, in each species (Fig. 3.3 (a)–(f), Table 3.1) [11]. It can also be noticed that, the base part of the water droplet shape is not perfectly flat, but forms curvy patterns with side-ends supported by the polygonal arms. For conducting CA experiments on flat surfaces, large sized drops are normally not considered in order to avoid the influence of the atmospheric pressure. Moreover, the size of the drop is kept smaller than the water capillary length (~2.5 mm) in order to avoid gravitational effect at large [12]. Since extremely small drops may get entrapped by the microstructure of bumpy rough surfaces, the CA measurements are dealt with drop sizes of comparable radii (~2.5 mm). A higher CA response of the distal part is due to the fact that, the region comprises of a sufficiently large number of microstructural polygonal units, as compared to the central and basal parts, and when all are covered with the water droplets of similar size. Earlier, it has been predicted that, a typical dragonfly wing would characterize a double surface roughness feature with fine and coarse segments [11]. Such a situation can arise only when there exists a tolerable variation in the surface roughness feature, which is quite different in the bound region (fine surface roughness) than that would be exhibited by the stiff fibrous stems (coarse roughness). Qualitatively, the surface roughness factor (r_φ) gives an idea about the overall roughness available in the specimen but offers no clue on how to isolate independent contributions accurately and precisely.

Table 3.1: The water CA, surface roughness factor and water solid fraction measured through different experiments and models. The values corresponding to dragonfly and damselfly cases are separated by a comma in the same row.

Part of the wing	Average CA (degree)	Roughness factor, r_φ (Wenzel)	Water-solid fraction, φ (Cassie-Baxter)
Basal	121(±1), 123(±1)	1.98, 2.10	0.65, 0.61
Central	127(±1), 124(±1)	2.33, 2.16	0.53, 0.60
Distal	133(±1), 130(±1)	2.62, 2.48	0.43, 0.48

3.4 Theoretical treatments on wettability conditions

The apparent water CA of a water drop on a typical rough surface can be explained either by using the Wenzel model or, the Cassie - Baxter model [13, 14]. The Cassie-Baxter model generally describes the suspended state of a water droplet on a pillar-like rough surface, where it does not fill up the grooves completely and air is likely to get entrapped beneath the water drop. Conversely, the Wenzel model is applicable to surfaces where the droplet makes its way into the grooves, and therefore signifies the collapsed state. Typically, the size of the water drop is larger than the average dimension of the microstructural elements and thus can accommodate many units. When the droplet is large as compared to the microroughness, the droplet is withdrawn by it and in that case, the Wenzel mode becomes more prominent [15]. According to Wenzel et al. [2,13], if θ and θ_w represent the respective water CAs of perfectly smooth and rough surfaces, then

$$cos\theta_w = r_\varphi cos\theta \qquad (3.1)$$

where, r_φ is the roughness factor and defined as the ratio between the actual surface area and the geometric projected area. Roughness factor, as the name suggests, gives an account as regards total unevenness present at the surface site. For a smooth surface, r_φ = 1. The Cassie-Baxter approach is a modified version of

the Wenzel model which accommodates the solid-water fraction, φ at the interface, and is given by:

$$\cos\theta_c = \varphi(1+\cos\theta) - 1 \qquad (3.2)$$

One can predict limiting value of the incremental CA by using the aforesaid equations independently and assuming $\theta = 105^\circ$ for a smooth surface (especially, made of chitin) as proposed by Holdgate in an elaborate work on insect cuticles [3]. These two models are regularly used by the research community while examining hydrophobic surfaces and immiscible interfaces of technological interest. The coexistence of these models has also been predicted on the same surfaces [16]. Even though the Wenzel model is best suited to the collapsed state and the Cassie-Baxter model to the suspended state, provided that the increment, $\Delta\theta < \theta$, at equilibrium, one can write,

$$\theta c = \theta w = \theta + \Delta\theta$$

From Wenzel model,

$$\cos\theta' = r\varphi\cos\theta$$

$$\cos(\theta + \Delta\theta) = r\varphi\cos\theta$$

$$\Rightarrow 1 - \frac{(\theta+\Delta\theta)^2}{2} = r_\varphi\left(1 - \frac{\theta^2}{2}\right)$$

$$\Rightarrow \frac{1-\theta^2}{2-\theta\Delta\theta} = r_\varphi\left(1 - \frac{\theta^2}{2}\right)$$

$$\Rightarrow \theta\Delta\theta = \left(1 - \frac{\theta^2}{2}\right)\left(1 - r_\varphi\right)$$

$$\Rightarrow \Delta\theta = \left(\frac{1}{\theta} - \frac{\theta}{2}\right)\left(1 - r_\varphi\right) \qquad (3.3)$$

From C-B model ,

$$\cos(\theta + \Delta\theta) = \varphi(1 + \cos\theta) - 1$$

$$\Rightarrow 1 - \frac{(\theta+\Delta\theta)^2}{2} = \varphi\left(1 - \frac{\theta^2}{2}\right) - 1$$

$$\Rightarrow 2 - \theta^2 - 2\theta\Delta\theta = \varphi(4 - \theta^2) - 2$$

$$\Rightarrow (4 - \theta^2) - 2\theta\Delta\theta = \varphi(4 - \theta^2)$$

$$\Rightarrow \Delta\theta = \frac{(4-\theta^2)(1-\varphi)}{2\theta} \qquad (3.4)$$

Here, Eqs. (3.3) and (3.4) are derived by expanding $\cos\theta$ (using Taylor's equation) in each of the Eqs. (3.1) and (3. 2) and by neglecting higher order terms

for the sake of convenience. For a very small increment in CA, *i.e.*, for $\Delta\theta < \theta$, one can find a relation between r_φ and φ expressed by:

$$r_\varphi = \frac{2-\varphi\,(4-\theta^2)}{\theta^2-2} \qquad (3.5)$$

and thus we obtain,

$$r\varphi = -0.47\varphi + 1.47, \qquad (3.6)$$

with θ=105^o, for a smooth surface and considering in radian units. We speculate that, the above expression is valid only up to a $\Delta\theta_{\max}$ of 10.1^o. As shown in the lower panel of Figure 3.4, the equation (3.6), could give a straight line feature and with a negative slope. Apparently, the surface roughness drops off slowly with an increasing value of the water-solid fraction, with r_φ=1.47 when φ=0, (rough surface) and r_φ=1 when φ =1 (smooth surface). On the other hand, through repeated experiments on the basal, central and distal specimens, we found $\Delta\theta$ values as high as ~31^o (Table 1). Using different data sets of measured CAs and employing Wenzel and Cassie-Baxter models independently to each part, r_φ and φ could be evaluated and their dependency can be established for a given wing-type (Fig. 3.4(b-d)). From actual data, the dragonfly and damselfly wings, infact, follow empirical relationship between these parameters, represented by:

$$r_\varphi^{dg} = -2.91\varphi + 3.88 \quad \text{(dragonfly)} \qquad (3.7)$$
$$r_\varphi^{dm} = -2.81\varphi + 3.83 \quad \text{(damselfly)}$$

Apparently, the wings characterize similar trends, but with a slope variation close to 4%. We anticipate that, many flies belonging to *Odanata* order would follow this trend and provided that, $\Delta\theta$ is large. In a recent work, the wettability of *Odanata* species was shown to exhibit a strong dependency on the amount of epicuticular waxes [17]. In principle, roughness factor cannot be in isolation from the solid-water fraction though the former largely rely on the geometrical construction, while the latter on the efficiency of adhesion. While mimicking

natural surfaces of biological origin, their interrelation could help immensely in the construction of artificial hydrophobic surfaces with desired wettability.

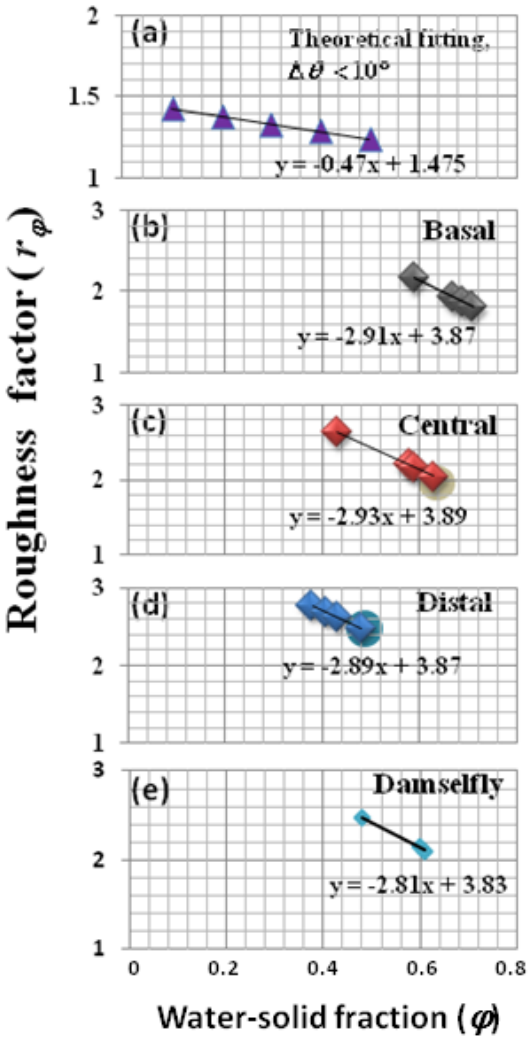

Table 3.2: Variation of roughness factor with solid-water fraction (theoretical)

φ	r_φ
0.1	1.43
0.2	1.38
0.3	1.33
0.4	1.29
0.5	1.24

Figure 3.4: The response of surface roughness factor vs. water-solid fraction in the (a) theoretical framework, and experimental results obtained from the (b) basal (c) central, and (d) distal parts of the dragonfly hind wing (e) damselfly, (right side) table 3.2 shows the values of roughness factor with varying water-solid fraction theoretically.

In this regard, not only dimension, but also ordering and shape of the inbuilt microstructural networks would play a deterministic role on the behaviour of the surface structure. Accordingly, we have observed altered de-wetting response through (CAs) on moving from the basal region to the extreme end-part. Secondly, the distribution of oblate-shaped nanostructures was seen to vary substantially as one goes from the basal to the distal region and more so that make-up the fibrous boundaries (Fig. 3.2(B)). The empirical relations, as highlighted in equation (3.7) are believed to alter for other *Odanata* species. This is because; the density of the nano-oblates within a bound region is capable of manifesting the strength of wettability when a water droplet comes in contact with the local surface structure. In the present case of the dragonfly wing, the reason behind a higher CA and hydrophobic response of the distal region is chiefly due to the availability of large number of polygonal units and high packing density of nanoscale chitinous oblates entrapped within a unit/compartment.

3.5 Reflectance characteristics of the hindwings and contributory roles of surface roughness

Fig. 3.5(a) depicts a series of reflectance spectra corresponding to the basal, distal and edge parts of the dragonfly hindwing. The respective microstructural micrographs are shown as side-view on the right hand side of the spectra. The semi-transparent specimens gave multi- reflectance peaks in the visible region apart from a distinct peak located at ~275 nm due to the abundant chitinous material present in the wing specimens [18, 19]. The peak at ~370 nm is relatively broad and asymmetric for both the basal and distal parts (Fig. 3.5(a)). Upon deconvolution through multi-peak Gaussian curve fitting on the basal and distal parts, we obtained two additional peaks located at ~422 nm and ~494 nm. It may be worth mentioning here that, the reflectance in the region 400-500 nm is generally attributed to the presence of carotenoid, and therefore, the dip located at ~460 nm can be ascribed to the absorption response of β–carotene [19]. The

overall reflectance response, is relatively stronger for the distal part than the basal region. As one makes a transition from the basal to the distal region, the microstructural parameter would decrease (and nanostructure roughness increase) [11], which results in a higher r_{φ}, and higher water CA. We anticipate an improved reflectance response in the distal region owing to the availability of densely packed nano-oblate light scatterers beneath the cuticle. Nevertheless, any departure from the arrangement and periodicity of microstructural network introduces heterogeneity into the system and might suppress the reflectance response with increasing wavelength. Consequently, in the long wavelength regime, the reflectance is substantially repressed both for the basal and distal parts. Earlier the nature of the reflectance spectra has been extensively studied to unravel pigmentary and structural effects in butterflies [20, 21, 22]. Nanostructure surface mediated wettability as well as bifunctional characteristics, such as, anti-reflection property and super-hydrophobic response of *Cicada* wings have also been demonstrated in earlier works [23, 24].

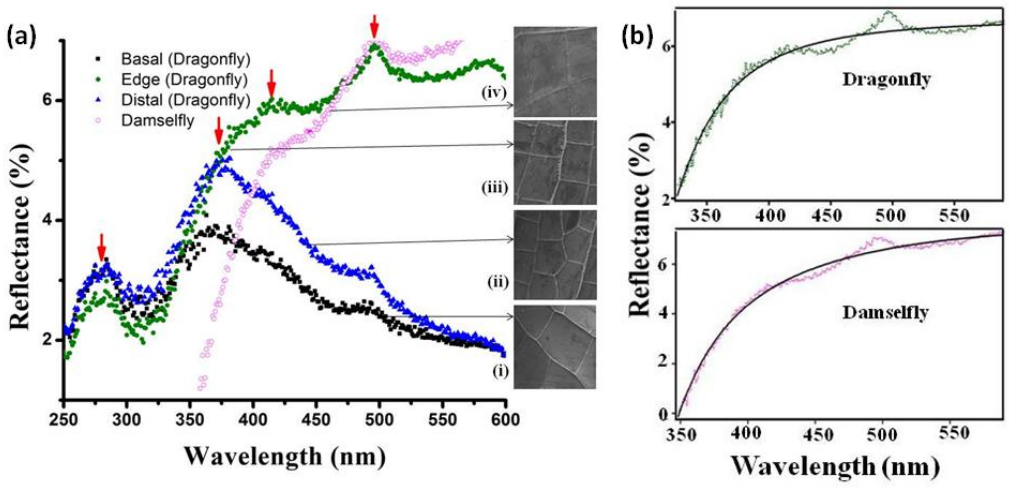

Figure 3.5: (a) UV–vis reflectance spectra of the basal, edge and distal parts of the hind-wing of the dragonfly. As for the damselfly wing, response due to the edge-specimen only is presented. (b) The curve fitting features of the reflectance curves of the edge parts.

Unlike basal and distal parts, the edge- part of the dragonfly hind wing exhibited a much stronger reflectance feature, particularly in the long wavelength regime. It may be noted that, the edge- part typically comprises of highly ordered, rectangular (500 μm x 700 μm) microstructural units without any triple junction build up. It is worth mentioning here that, a higher reflectance is realized when light scattered from the concerned interfaces appear in phase. This is possible when every surface layer present in the 2D chitinous plane has an optical thickness comparable to that of a quarter wavelength ($\lambda/4$). While realizing the average tip-end diameter of the randomly distributed chitin oblates and rods as approximately 125 nm (Fig. 3.2(A)(b)), significant coherent scattering is expected to occur from these nano-structured elements, giving rise to a characteristic peak maximum at ~494 nm. An enhanced reflectance response may also be caused by multilayer interference occurring through thin chitinous elements and air-gaps. In this regard, existence of nearly 2-3 thin layers has been observed in the wings of a similar insect type, namely *Calopteryx Japonica* [25]. However, an overall growing reflectance trend with increasing wavelength, as noticed in the edge-specimen, calls for analogy in terms of roughness limited scattering. The reason behind selecting this edge specimen is that the edge-subpart would exist in every main-part of the wings, be it basal, central or distal. Moreover, the edge-part is free from the diverse microstructure types and is made up of only rectangular elements spread uniformly along the specimen boundary.

It is worth noting that, light scattering from a surface structure is characterized either by specular reflection or inelastic diffusive process. In order to assess reflectance response of a rough surface, here, one can define root mean square roughness, r_μ, as the root mean square deviation of the surface-top from the mean surface level. In the past, the specular reflectance at normal incidence for a polished conducting surface was proposed by Davies *et al.*[26, 27]:

$$R = R_0 \, exp\,[-(4\pi r_\mu)^2/\lambda^2], \qquad (3.8)$$

where, R_0 is the reflectance of the perfectly smooth surface of the same material, λ is the incident light wavelength and that, λ and r_μ are measured in the unit of length. It is worth mentioning here that, r_μ has a characteristic dimension of length, but r_φ is a dimensionless entity (being a ratio of the actual surface area to the projected area). For naturally occurring samples, as in the present case, the overall surface scattering is mediated via two scattering principles: surface scattering (reflectance) and sub-surface volume scattering. The edge-specimens of the dragonfly and blueriver damselfly wings, while being comprised of periodic arrangement of microstructural units, offered growing reflectance trends with increasing wavelength (Fig. 3.5(b)), we intended to determine associated roughness parameters in the aforesaid specimens. The dragonfly wing essentially gives a progressive reflectance curve, featuring a steep rise beyond 370 nm and exhibiting additional peak maxima at ~422 nm. The reflectance peak maxima, positioned at ~494 nm, are common features of both the dragonfly and the damselfly edge-specimens (Fig. 3.5(b)). As the specimen of the damselfly wing exhibited a rapid fall in the low wavelength regime, the edge-specimen, in this case might be a strong absorber of UV light (< 350 nm). The relative strength of reflectance corresponding to ~494 nm and 370 nm peaks, both for basal and distal segments of the dragonfly wing, is close to 0.7, which shoots up to ~1.4 in the edge-specimen (Fig. 3.5(a)). In other words, the association of periodic rectangular structures and inner surface irregularities present in the edge-part are chiefly responsible for growing reflectance characteristics at longer wavelengths. In particular, plentiful nano-bumps would experience significantly high sub-surface volume scattering and hence, contribute largely to the overall reflectance response in the extended visible region. By employing *IgorPro*® software, the reflectance data of the edge parts were subjected to appropriate curve fitting over a broad wavelength range, while ensuring a minimal chi-square value (Fig. 3.5(b)). The overall spectra would follow an associated exponential curve fitting of the form given by:

$$R = R_0 [1 - exp(-\lambda^2/r_{\mu w}^2) - exp(-\lambda^4/r_{\mu s}^4)], \qquad (3.9)$$

which is quite different from the representative feature of polished conducting surfaces given in equation (3.8). Here, $r_{\mu s}$ and $r_{\mu v}$ characterize respective surface roughness contributions associated with the surface reflectance and the sub-surface volume scattering; respectively. Consequently, as for the dragonfly edge specimen, the respective roughness parameters are estimated as, $r_{\mu s}$~ 368.5 nm and $r_{\mu v}$~ 241 nm. As for damselfly, the respective parameters are ~ 372 nm and ~ 280 nm. The submicron roughness, $r_{\mu s}$ is comparable to ~370 nm peak maxima and is believed to have originated from the overall surface make up of the chitin-oblate assemblies undergoing specular reflection. In contrast, $r_{\mu v}$ is a consequence of diffusive scattering aroused via curved surfaces and interfaces of the naturally occurring chitin oblates. Not surprisingly, it is the latter surface parameter which largely influences water repellency and must be linked to r_{φ} discussed in earlier section.

In order to deal r_{φ} and $r_{\mu v}$ on equal footing, $r_{\mu v}$ needs to be standardized with the two strong peak maxima which characterize carotenoid support, *i.e.*, λ_m=422 nm and 494 nm. These are the characteristic wavelength meant for coherent scattering events. Therefore, in this case, roughness factor can be recalled as, $r_{\mu v}/ = \lambda_m / r_{\mu v}$. Consequently, the dragonfly specimen can have $r_{\mu v}/$ in the range of 1.75 and 2.05. The damselfly specimen has $r_{\mu v}/$ between 1.5 and 1.76. When these values are fitted for r_{φ} in the empirical equations (3.7), we noticed that, the effective water-solid fraction, φ takes a value between 0.62 and 0.73 (shadow area, Fig. 3.4). This is indicated by shadowed circles in the tail-end response of the basal and central-parts of the dragonfly hind-wing investigated (Fig. 3.4).

3.6 Concluding remarks

The hydrophobic and reflectance responses of two *Odanata* species have been demonstrated through the CA measurements and reflectance studies; respectively. A simplified model is worked out assuming Wenzel and Cassie-Baxter models to hold simultaneously. In both the dragonfly and damselfly

wings, the distal parts were found to be more hydrophobic than the other parts owing to the exhibition of a relatively higher CA in the distal part. We anticipate an improved surface structure in this part owing to the availability of relatively densely packed chitinous nanofibrils. Appropriate empirical relations connecting r_φ and φ have been revealed for specimens under study. The overall reflectance is observed to be stronger in the distal part than the basal counterpart. In contrast, the edge-parts displayed growing reflectance trends while featuring broadened peak maxima at ~422 nm and 494 nm, for both the dragonfly and damselfly wing-parts. The analysis of reflectance spectra of the edge specimens provided a clue to interrelate sub-micron surface roughness with the roughness factor, and consequently with the de-wetting (hydrophobic) response. In the absence of repetitive measurements of CA and reflectance response from various parts of the blue-river damselfly wing, a connection could not be established with certainty. This is because; the wing span was not only thin but also mechanically unstable for handling purposes. It was extremely difficult to extract complete diffusive scattering occurring within a confined geometry, as localized heating is likely to alter dislodge the internal build up. In this backdrop, a direct connection between the overall reflectance feature and wetting property may be realistic with advanced versions of reflectance spectroscopes including polarization dependency and total internal reflection aspects into account. The scope of interrelating optical window and microstructure roughness can be widened further to unravel bifunctional features in a more precise manner, which is underway.

References

[1] Song, F., Xiao, K.W., Bai, K., Bai, Y.L. Microstructure and nanomechanical properties of the wing membrane of dragonfly. *Materials Science and Engineering*, A475:254–260, 2007.

[2] Wenzel, R.N. Resistance of solid surfaces to wetting by water. *Industrial and Engineering Chemistry*, 28:988-994, 1936.

[3] Holdgate, M.W. The wetting of insect cuticles by water. *Journal of Experimental Biology*, 32:591-617, 1955.

[4] Parker, A.R., Lawrence, C.R. Water capture from desert fogs by a Namibian beetle. *Nature*, 414:33–34, 2001.

[5] Feng, X.-Q., Gao, X., Wu, Z., Jiang, L., Zheng, Q.-S. Superior Water Repellency of Water Strider Legs with Hierarchical Structures: Experiments and Analysis. *Langmuir*, 23:4892-4896, 2007.

[6] Bormashenko, E., Bormashenko, Y., Stein, T., Whyman, G., Bormashenko, E. Why do pigeon feathers repel water? Hydrophobicity of pennae, Cassie–Baxter wetting hypothesis and Cassie–Wenzel capillarity induced wetting transition. *Journal of Colloid and Interface Science*, 311:212-6, 2007.

[7] Cassie, A.B.D. Contact angles. *Discussions of the Faraday Society*, 3:11-16, 1948.

[8] https://indiabiodiversity.org/species/show/276041

[9] Smith, C.W., Herbert, R., Wootton, R.J., Evans, K.E. The hind wing of the desert locust (Schistocerca gregaria Forskal). II. Mechanical properties and functioning of the membrane. *Journal of Experimental Biology*, 203:2933-2943, 2000.

[10] Feng, X.-Q., Gao, X., Wu, Z., Jiang, L., Zheng, Q.-S. Superior Water Repellency of Water Strider Legs with Hierarchical Structures: Experiments and Analysis. *Langmuir*, 23: 4892-4896, 2007.

[11] Gao, C.-Y., Meng, G.-X., Li, X., Wu, M., Liu, Y., Li, X.-Y., Zhao, X., Lee, I., Feng, X. Wettability of dragonfly wings: the structure detection and theoretical modelling. *Surface Interface Analysis*, 45:650-655, 2013.

[12] Diana, A., Castillo, M., Brutin, D., Steinberg, T. Sessile Drop Wettability in Normal and Reduced Gravity. *Microgravity Science and Technology*, 24:195-202, 2012.

[13] Wenzel, R.N. Surface Roughness and Contact Angle. *Journal of Physical and Colloid Chemistry*, 53:1466-1467, 1949.

[14] Cassie, A.B.D. Contact angles. *Discussions of the Faraday Society*, 3:11-16, 1948.

[15] Nakajima, A. Design of hydrophobic surfaces for liquid droplet control. *NPG Asia Materials*, 3:49-56, 2011.

[16] Giacomello, A., Meloni, S., Chinappi, M., Casciola, C.M. Cassie−Baxter and Wenzel States on a Nanostructured Surface: Phase Diagram, Metastabilities, and Transition Mechanism by Atomistic Free Energy Calculations. *Langmuir*, 28:10764-10772, 2012.

[17] Nguyen, S.H., H.K. Webb, Hasan, J., M.J. Tobin, D.E. Mainwaring, P.J. Mahon, R. Marchant, R.J. Crawford, E.P. Ivanova, Vib. Spectrosc. 75 (2014) 173.

[18] Stoddart, R., Cadusch, P.J., Boyce, T.M., Erasmus, R.M., Comins, J.D. Optical properties of chitin: surface-enhanced Raman scattering substrates based on antireflection structures on cicada wings. *Nanotechnology*, 17:680-686, 2006.

[19] Boruah, R., Nath, P., Mohanta, D., Ahmed, G.A., Choudhury, A. Photonic Properties of Butterfly Wing Infiltrated with Ag-Nanoparticles. *Nanoscience Nanotechnology Letters*, 3: 458-462, 2011.

[20] Wilts, B.D., Pirih, P., Stavenga, D.G. Spatial reflection patterns of iridescent wings of male pierid butterflies: curved scales reflect at a wider angle than flat scales. *Journal of Comparative Physiology A*, 197:987-997, 2011.

[21] Kinoshita, S. Structural Colors in the Realm of Nature, World Scientific Publishing, Singapore, 2008, pp. 112.

[22] Ding, Y., Xu, S., Wang, Z.L. Structural colors from Morpho peleides butterfly wing scales. *Journal of Applied Physics*, 106:074702, 2009.

[23] Dellieu, L., Sarrazin, M., Simonis, P., Deparis, O., Vigneron, J.P. A two-in-one superhydrophobic and anti-reflective nanodevice in the grey cicada Cicada orni (Hemiptera). *Journal of Applied Physics*, 116: 024701, 2014.

[24] Sun, M., Watson, G.S., Zheng, Y., Watson, J.A., Liang, A. Wetting properties on nanostructured surfaces of cicada wings. *Journal of Experimental Biology*, 212: 3148–3155, 2009.

[25] Hariyama, T., Hironaka, M., Horiguchi, H., Stavenga, D.G., Kinosita, S., Yoshioka S. (Eds.), Structural Colors in Biological Systems, Osaka Univ Press, Osaka, 2005, p. 153.

[26] Davies, H. The reflection of electromagnetic waves from a rough surface, *Proceedings of the IEEE*, 101:209-214, 1954.

[27] Bennett, H.E., Porteus, J.O. Relation Between Surface Roughness and Specular Reflectance at Normal Incidence. *Journal of the optical society of America*, 51:123-129, 1961.